Supporting Information

NOx Selective Catalytic Reduction (SCR) on Self-Supported V-W-doped TiO_2 Nanofibers

D. Marani[†a], R. H. Silva[a], A. Dankeaw[a], K. Norrman[a], R. M. Larsen Werchmeister[b], D. Ippolito[a], M. Gudik-Sørensen[a], K. Kammer Hansen[a], V. Esposito[a]

[a] Department of Energy Conversion and Storage, Technical University of Denmark (DTU), Frederiksborgvej 399, Roskilde, DK-4000, Denmark
[b]Department of Chemistry, Technical University of Denmark (DTU), Kemitorvet, Building 207, Kgs. Lyngby, 2800, Denmark
†Corresponding author, e-mail address: debora.marani3@gmail.com

In *Table S1* the characteristics of the cations used in the preparation of the titania-doped nanofibers are indicated. Both vanadium (V^{+5}) and tungsten (W^{+6}) are expected to substitute the titanium (Ti^{+4}) in the titania lattice, producing a solid solution. This is expected to happen because of similar radii for the involved cations [1].
The differences in the electronegativity (expressed as Pauli scale), as discussed in the paper, alter the electronic structure of the titania lattice.

Elements	Ionic Radii (nm)	Electronegativity (Pauli scale)	Standard Reduction Potentials (V)
Titanium (Ti^{4+})	0.0605	1.54	Ti^{+4}/Ti^{+3}=0.00
Tungsten (W^{6+})	0.0600	2.36	W^{+6}/W^{+5}=-0.03
Vanadium (V^{5+})	0.0540	1.63	V^{+5}/V^{+4}=0.96

TableS1-Characteristics of the elements used.

In *Table S2* the composition, the grains´ sizes (obtained from XRD pattern applying the Scherrer equation and the specific surface area (SSA) for all the developed titania-based nanofibers are listed.

Sample	Composition				Grains Sizes (nm)	Surface Specific Area (m^2/g)
	Ac/Ti	TiO_2	V_2O_5	WO_3		
TiO_2	10	100	/	/	32.41	24.27
V-TiO_2	10	97	3	/	29.58	29.17
W-TiO_2	10	95	/	5	27.78	36.14
V-W-TiO_2	10	92	3	5	27.60	37.69
V-W-TiO_2	5	92	3	5	27.56	59.52
V-W-TiO_2	2	92	3	5	27.80	57.44

Table S2-Compositions, grains size and SSA for all the materials developed.

Results and discussion

Thermal gravimetric analysis

The conditions for the calcination were fixed based on the thermal gravimetric analysis results. As indicated in Figure S1, a weight loss of around 65%, associated with the decomposition of organics, is observed at temperature lower than 450 °C. For higher temperature no variation in the weight is detected.

Accordingly, a calcination temperature of 500 °C was then used to remove any organics from the ceramic nanofibers.

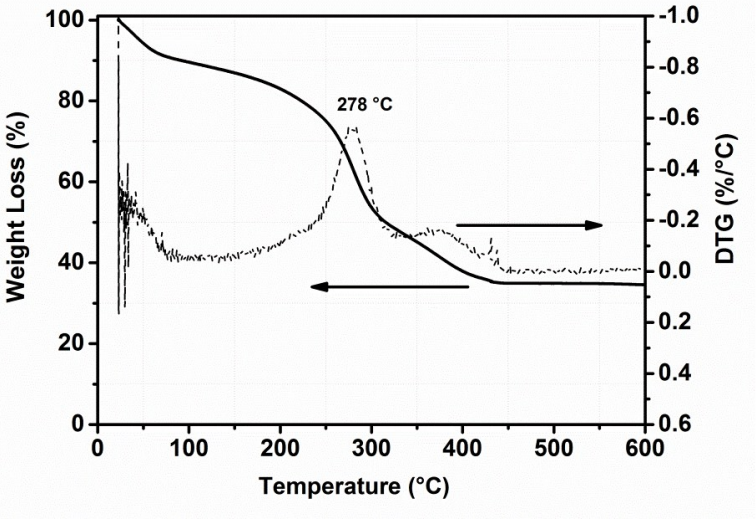

Figure S1-TGA/DTG profile for the V-W-TIO_2 nanofibers.

Effect of acetic acid content on nanofibers morphology-SEM characterization

The effect of the acetic acid content on the nanofiber morphology was investigated. Figure S2 shows the morphology features for full compositions samples obtained at [Ac]/[Ti]=2, 5, and 10. A clear and gradual improvement in the fibre morphology (diameter homogeneity) is observed as the [Ac]/[Ti] increase. The material prepared at [Ac]/[Ti]=5 already exhibits a homogeneous morphology. However, superior morphological features, in terms of extremely highly homogenous distribution of the nanofiber diameters, are obtained for the material prepared at [Ac]/[Ti]=10 (diameters in the range of 80-120 nm). The trend in the nanofibers morphology can be associated to the stabilizing effect of the acetic acid towards the hydrolysis/condensation process for the alkoxides involved. The use of a ligand (*e.g.* acetic acid) has been comprehensively proven to stabilize the central atom with the formation of stable molecular precursors (*e.g.* complexes) whose stability and dimension depends on the reciprocal concentration of alkoxides and ligand [3-5]. The formation of a stoichiometric stable compounds (*e.g.* $Ti(OR)_2(Acet)_2$) when [Ac]/[Ti]=2 has been suggested, whereas at higher concentration, poly-nuclear and stable complexes are generated via bridging mechanism with a consequent slowdown of the sol-gel process. At even higher concentrations, the precipitation of oxo-acetate was obtained [3, 4].

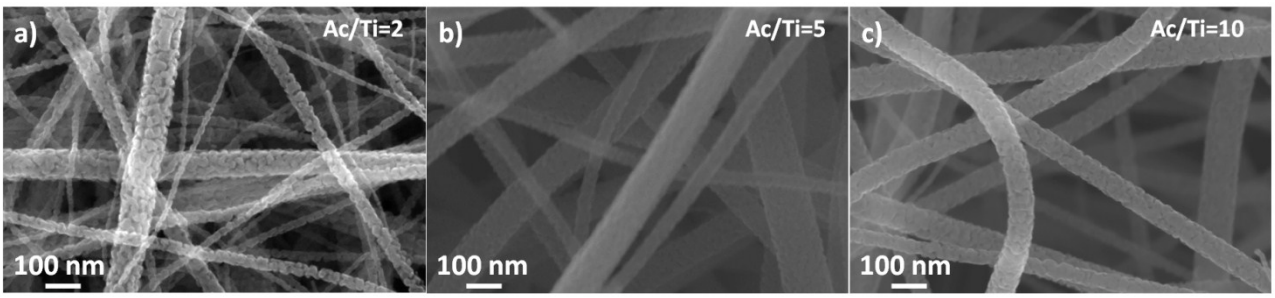

Figure S2-SEM pictures of nanofibers prepared at increasing amount of acetic acid.

In the current work, solutions at [Ac]/[Ti] higher than 10 were also prepared but were not electro-spun as a gelatinous precipitate was observed few hours after the preparation.
The larger SSA that characterized the nanofibers prepared at [Ac]/[Ti]=2 and 5 is consistent with the morphological features observed. Indeed, the lower the diameter of nanofibers, the larger the SSA is expected. Accordingly, only the complete series of materials (from pure titania to the full doped composition) at [Ac]/[Ti]=10 was then prepared.

XRD analysis

An effect of the addition of dopants on the crystallographic phase of the materials was clearly observed. As discussed in the main paper, the addition of the dopants favours the anatase phase inhibiting the formation of the rutile, that is observed together with the anatase only in the pure TiO_2 nanfibers. The crystallinity, the phase structure and crystal parameters of pure and doped-TiO2 samples were investigated by analysing the XRD pattern.
The average size of the grain was determined using the Debye–Scherrer equation [2]

$$Average\ grain\ size = \frac{0.9\,\lambda}{\beta \cos\theta} \quad \text{Equation S1}$$

where, λ is the wavelength of the incident X-ray radiation (0.154 nm), β is the broadening of the diffraction line measured at half of its maximum intensity in radians, and θ is the Bragg's diffraction angle. The trend for the average crystallite sizes are reported in *Table S3.*

The lattice parameters were estimated considering the tetragonal crystal structure for the TiO_2, with thus the lattice parameters following the conditions a = b ≠ c (and α = β = γ=90°). The lattice parameters were calculated by applying the standard formula for the tetragonal system [ref]:

$$\frac{1}{d_{hkl}^2} = \frac{h^2 + k^2}{a^2} + \frac{l^2}{c^2} \quad \text{Equation S2}$$

where *d* is the interplanar spacing, *h*, *k*, *l* represents the Miller indices of the planes and *a*, *b* and *c*, the lattice parameters. The results obtained are reported in *Table S3*. The non-dimensional parameter c/a is also indicated together with the cell volume.

The spacing corresponding to the planes (101) and (200) of the anatase phase were determined by applying the Braggs´s equation:

$$d_{hkl} = \frac{n\,\lambda}{2\,sen\theta} \quad \text{Equation S3}$$

where d is the spacing of the crystal planes, *(h*, *k*, *l)* are the Miller indices, *n* is a positive integer, λ is the wavelength of the incident X-ray radiation (0.154 nm), θ is the Bragg´s diffraction angle*.* The results obtained are reported in *Table S3*.

Sample	Average grains sizes (nm)	d(101) anatase	d(200) anatase	Lattice Parameters			
				a=b (Å)	C (Å)	c/a	Cell volume (Å³)
TiO_2	32.41	3.519	1.894	3.788	9.510	2.511	136.474
V-TiO_2	29.58	3.522	1.895	3.790	9.549	2.518	137.021
W-TiO_2	27.78	3.530	1.898	3.796	9.608	2.528	138.330

V-W-TiO_2	27.60	3.525	1.897	3.793	9.536	2.514	137.222

Table S3*-Structural parameters for the complete series of samples prepared at [ac]/[Ti]=10).*

Compared to the un-doped TiO_2, the addition of the dopants causes a slight shift toward higher diffraction angles for the XRD peaks of plan (101) and (200) as indicated in Fig. S3 and summarized in *Table S3*.
The estimated values of lattice parameters are consistent with those reported in literature (a_0=0.3785 nm, c_0=0.9513 nm, c/a=2.51 for anatase). The variation of lattice constants from the value indicates a distortion in the unit cell structure.

In Figure S3 the shift associated with the plane (101) and (200) of the anatase phase upon the addition of the dopant cations are indicated together with the variation of the lattice parameters of the unit cell.

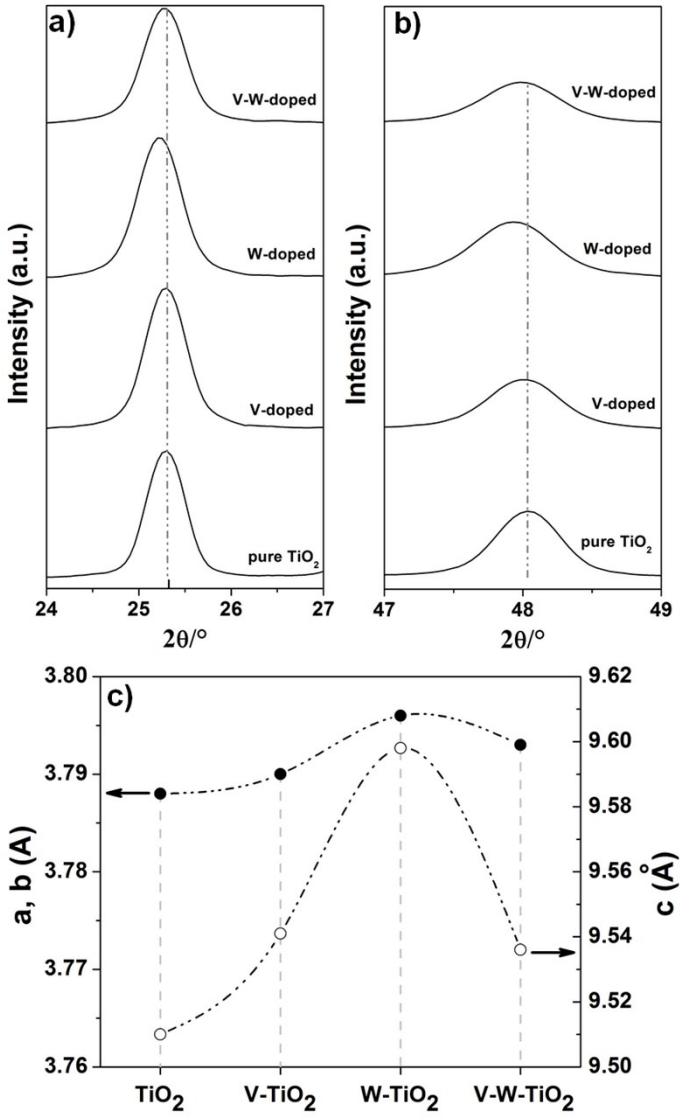

Figure S3-Shift of the diffraction angle associated with (a) plane (101) and (b) plane (200) of the anatase phase; (c) variation of the lattice parameters for the complete series of samples prepared at [Ac]/[Ti]=10.

X-ray photoelectron spectroscopy (XPS)

In the following relevant information resulting from the XPS analysis are reported for series of samples prepared at [Ac]/[Ti]=10.

In *Table S4* the binding energy (BE) associated with the relevant photo-electron peaks are indicated.

Sample	Oxygen BE (eV)		Titanium BE (eV)			Tungsten BE (eV)		Vanadium BE (eV)	
	O1s (Oα, lattice)	O1s (O_β, OH)	$Ti^{4+}2p_{3/2}$	$Ti^{4+}2p_{1/2}$	$Ti^{4+}3p$	$W^{+6}4f7$	$W^{6+}4f5$	$V^{4+}2p$	$V^{5+}2p$
TiO_2	529.60	531.70	458.10	463.90	/	/		/	/
V-TiO_2	529.60	531.90	458.10	463.80	/	/		515.70	516.70
W-TiO_2	530.00	531.60	458.90	464.60	37.6	35.90	37.90		
V-W-TiO_2	529.80	531.80	458.30	464.10	37.3	35.90	37.80	516.20	517.20

Table S4-Binding energy associated to the photo-electron lines of interest from XPS analysis.

In *Table S5* the surface atomic composition together with the relative increment of the chemi-adsorbed oxygen (-OH) and the variation of the V^{4+}/V^{5+} are listed. For the full doped sample (V-W-TiO_2), the surface atomic percentage for tungsten and vanadium (within the experimental errors) are consistent with the fixed composition for which WO_3/V_2O_5 molar ratio is roughly fixed at 1. This is likely an indication that during the electrospinning process, the active materials (WO_3 and V_2O_5) are generated onto the nanofibers surface.

Sample	Surface atomic percentage (%)				$\frac{O_\alpha}{O_\alpha + O_\beta}$	V^{4+}/V^{5+}
	Oxygen	Titanium	Tungsten	Vanadium		
TiO_2	76.3 ± 0.5	23.7 ± 0.5	/	/	0.21	/
V-TiO_2	74.6 ± 0.2	23.1 ± 0.2	/	2.4 ± 0.2	0.15	0.19
W-TiO_2	75.5 ± 1.1	22.5 ± 1.2	2.0 ± 0.2	/	0.14	/
V-W-TiO_2	77.3 ± 1.0	19.0 ± 1.2	1.3 ± 0.2	2.4 ± 0.2	0.21	0.89

Table S5-Surface atomic percentage, $O_\alpha/(O_\alpha+O_\beta)$ and V^{4+}/V^{5+} ratio for the developed nanofibers materials.

In Figure S4*a* the peak area for the Ti^{4+} 2p photo electron signals from the pure titania to the full composition material is indicated. A progressive decreasing of the area is observed as consequence of the substitution into the lattice. Interestingly, for V-TiO_2 and W-TiO_2 samples similar values for the peak area are obtained in agreement with the atomic composition indicated in Table S5 for Titanium. Eventually, the lowest value of area was observed for the full composition sample (V-W-TiO_2). In Figure S4*b*, V^{4+}/V^{5+} is then indicated.

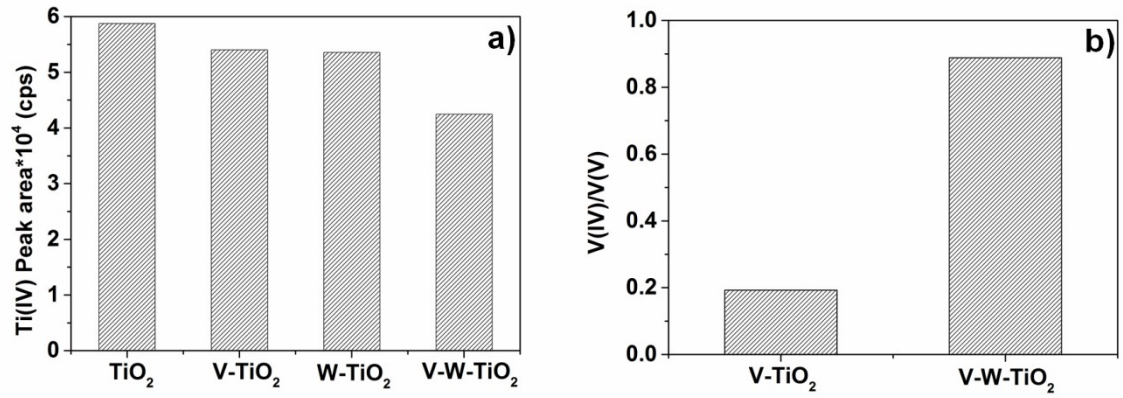

Figure S4-(a) Ti^{4+} peak area for the complete series of samples ([Ac]/[Ti]=10), and (b) V^{4+}/V^{5+} for the two samples containing vanadium as dopant element.

SCR performances

In the *Table S6* the Arrhenius fitting parameters together with the activation temperature (T_a) for the differently doped nanofibers (V-TiO_2 and V-W-TiO_2) prepared at [Ac]/[Ti]=10 are indicated. As discussed in the manuscript, similar values of activation energy (E_a) within the experimental error), were obtained for the materials. By contrast, a huge difference in the pre-exponential factor (A) is obtained indicative of a larger amount of active sites (V^{4+}-OH) for the V-W-TiO_2.

Sample	Activation Energy, E_a (KJ/mol)	Pre-exponential Factor, A	Activation Temperature, T_a (°C)
V-TiO_2	18.70 ± 2.37	$2.86*10^3 \pm 0.15*10^3$	350
V-W-TiO_2	16.56 ± 1.98	$6.07*10^3 \pm 0.69*10^3$	320

Table S6- Arrhenius fitting parameters for the doped titania based nanofibers prepared at [Ac]/[Ti]=10.

References

1 R.D. Shannon, *Acta Cryst.*, 1976, **A32**, 751-767.
2 P. B. Nair, V.B. Justinvictor G. P. Daniel, K. Joy, K.C. J. Raju, D. D. Kumar, P.V. Thomas; *Progress in Natural Science: Materials International* 2014, **24**, 218–225.
3 S. Doeuff, M. Henry, C. Sanchez, J. Livage, *Journal of Non-Crystalline Solids*, 1987, **89**, 206-216.
4 S. Doeuff, M. Henry and C. Sanchez, *Mat. Res. Bull.*, 1990, **25**, 1519-1529.
5 R. Parra, M. S. Góes, M. S. Castro, E. Longo, P. R. Bueno, J. A. Varela, *Chem. Mater.*, 2008, **20**, 143–150.